Audio Engineering Society

Convention Paper

Presented at the 126th Convention
2009 May 7–10 Munich, Germany



# An Alternative Ambisonics Formulation: Modal Source Strength Matching and the Effect of Spatial Aliasing

Franz Zotter[1], Hannes Pomberger[1], and Matthias Frank[2]

[1] *Institute of Electronic Music and Acoustics, University of Music and Performing Arts Graz, Austria.*

[2] *Student, Graz University of Technology, Austria.*

Correspondence should be addressed to Franz Zotter (zotter@iem.at)

**ABSTRACT**

Ambisonics synthesizes sound fields as a sum over angular (spherical/cylindrical harmonic) modes, resulting in the definition of an isotropically smooth angular resolution. This means, virtual sources are synthesized with outstanding smoothness across all angles of incidence, using discrete loudspeakers that uniformly cover a spherical or cylindrical surface around the listening area. The classical Ambisonics approach models the fields of these discrete loudspeakers in terms of a sampled continuum of plane-waves. More accurately, the contemporary concept of Ambisonics uses a continuous angular distribution of point-sources at finite distance instead, which is considerably easier to imagine. This also improves the accuracy of holophonic sound field synthesis and the analytic description of the sweet spot. The sweet spot is a limited area of faultless synthesis emerging from angular harmonics truncation. Additionally, playback with loudspeakers causes spatial aliasing. In this sense, the contemporary concept allows for a succesive consideration of the major shortcomings of Ambisonics: the limited sweet spot size and spatial aliasing. To elaborate on this, our paper starts with the solution of the nonhomogeneous wave equation for a spherical point-source distribution, and ends with a novel study on spatial aliasing in Ambisonics.

## 1. INTRODUCTION

Several spatial audio rendering techniques use different weights to distribute an acoustic source signal to pairs or triples of loudspeakers of the multichannel setup. Essentially, stereophony [1] and vector base amplitude panning (VBAP, [2]) use this well-known

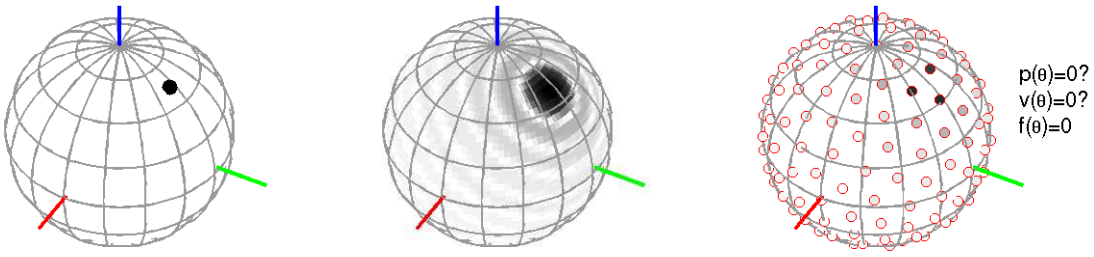


(a) Continuous distribution (b) Angularly band-limited distr. (c) Discretized distribution

Fig. 1: Illustration of a continuous point-shaped distribution on the sphere (a) and its angularly band-limited version (b). May a discretized distribution (c) physically correspond to sound pressure, radial sound particle velocity, or source strength to model a spherical sound reproduction system?

psychoacoustic effect, commonly referred to as phantom source [3]. Ambisonics in its simple form [4], as known to many live electronics technicians and electronic music artists, also distributes a source signal with different weights to loudspeakers, however with non-zero weights for most speakers. In an abstract sense, the source image created by the loudspeakers will resemble a point-source, which can be placed at a variable angle on the surface spanned by the reproduction system.

The background behind Ambisonics, the spherical sound field description, however, is mathematically more powerful than amplitude panning. It provides convergent wave field reproduction within a central listening area of limited size (sweet spot, [5, 6, 7, 8, 9, 10]). Ambisonics can be viewn as an alternative to wavefield synthesis, but restricts to spherical/circular geometries. In general, *distance coding* and the reproduction of directional sound sources [11] is feasible. Moreover, the mathematical fundamentals fully include the capture and synthesis of incident and radiating sound fields with spherical arrays [12, 13, 14, 15, 16, 17, 18, 19, 20, 21].

### 1.1. Introduction of Ambisonics

The classical Ambisonics approach relies on a plane-wave model representing the waves emitted by the playback loudspeakers [22]. This concept is very present to the Ambisonics enthusiasts. However, such a plane-wave model is neither accurate, nor does it really simplify the concept of Ambisonics. Also, the classical plane-wave Ambisonics slightly obscures the real reason for the sweet spot. It misleads to a simplification that the sweet spot would arise from the fact that plane-wave analysis and synthesis refers to one single point, only. Fortunately, as Ambisonics evolves, loudspeakers and virtual sources can be expressed in terms of point-sources [5, 23, 7, 9, 10, 24]. Newer literature on Ambisonics [6, 7, 8, 9] illustrates the two main reasons causing the sweet spot.

Firstly, Ambisonics limits the angular resolution to diminish the loss of directional information due to angular sampling, see Fig. 1 (a) and (b). It is a mathematical property that this limited resolution yields a reduced range of accurate sound field representation [7, 6, 8], the sweet spot, see Fig. 2 (a) and (b).

Secondly, angular sampling at discrete loudspeaker positions yields further limitations due to spatial aliasing, see Fig. 2 (c). This spatial aliasing strongly depends on the spherical/circular sampling strategy, and there has been only little investigation on its effect [23, 7, 25].

It is an important achievement of the newer literature on Ambisonics [7, 6] to have these two critical aspects seperated. However, literature severely lacks a practical characterization of how and where spatial aliasing affects Ambisonics.

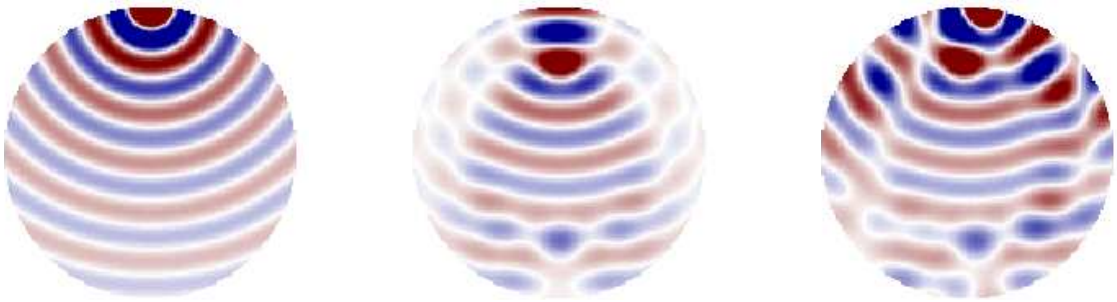

(a) Continuous (b) Angularly band-limited (c) Discretized

Fig. 2: The sound field of a point-source located at the boundary of a spherical/cylindrical region (a), changed by angular band-limitation (b), and subsequent reproduction with discrete sources (c).

## 2. THE PHYSICS OF AMBISONICS

To physically characterize Ambisonics, a naive idea (in analogy to [18]) is to think about an interior sound field reproduction using a spherical or cylindrical membrane or boundary, i.e. in mathematical terms: a *boundary condition* [26, 27].

But neither types of boundary conditions, sound pressure (Dirichlet) or radial sound particle velocity (Neumann) seem to be admissible. Both imply a reflective spherical/cylindrical boundary, causing pronounced spatial modes. Hence, frequencies associated with the modal zeros at the boundary, yield a numerically ill-posed *mode-matching* problem, cf. [6, 28].

One inconsistency of this idea is particularly easy to show. Assume to spatially sample the boundary condition for playback with discrete loudspeakers. Depending on the kind of boundary condition, either the sound pressure or the radial particle velocity must become zero on the segments between the sampling nodes, see Fig. 1 (c). High-quality electroacoustic playback facilities avoid this kind of reflective spherical/cylindrical surfaces, hopefully.

There is one concise answer to the question posed in Fig. 1: resynthesis is easiest described with discrete point-sources. This allows for unconstrained sound pressure and particle velocities between the discrete sources. Consequently, preceding discretization, it is consistent to assume a source strength distribution of infinitely many point-sources instead of sound pressure or sound particle velocity patterns. We describe this as the nonhomogeneous Helmholtz-equation[1], cf. [27], excited by a spherical/cylindrical source strength distribution. It can be shown that this source arrangement is capable of reproducing any homogeneous interior field. Within this context, recent literature uses the terms *single-layer potential* [9, 29] or *simple-source approach* [7].

The limitation of the angular resolution before discretization of the source strength distribution, depicted in Fig. 1 (a) and (b), unfavorably causes a limited size of the listening area, see Fig. 2 (b). However, this angular smoothing also limits the loss of directional information for the playback with discrete sources, see Figs. 1 (c) and 2 (c). This is the reason for the celebrated smoothness of Ambisonics.

Note that the typical Ambisonics approach does not directly sample the desired source strength distribution to obtain the discrete source signals. Instead of sampling in the space-domain, the continuous desired distribution is compared with the discretized distribution in the modal spherical/circular harmonics domain. *Matching* of these two distributions explicitly requires inversion of a system of equations (matrix inversion) to obtain accurate results.

Despite its similarity to the classical Ambisonics *mode-matching*, the hereby employed *modal source strength matching* does not suffer from ill-posedness of restricted modal frequencies.

[1] The Helmholtz equation $(\Delta + k^2)\, p = 0$ is the wave equation in the frequency domain.

The new perspectives on Ambisonics shall provide an easier understanding of the principles of Ambisonics, and yield an improvement in the concept of high-level strategies like *distance coding* [30] and possible future extensions of Ambisonics sound field reproduction. It is furthermore nice to see that no explicit integral formulation (Kirchhoff-Helmholtz-equation, simple-source approach, or single-layer potential) is required as a direct solution is available.

The following sections consider a spherical geometry only. However, a reformulation to circular-cylindrical geometry can be found easily.

## 3. A CONTINUOUS SPHERICAL POINT-SOURCE DISTRIBUTION

On a sphere with constant radius $r_l$, the dependency on the two space angles, azimuth $\varphi$, zenith $\vartheta$, can be expressed as a Cartesian unit vector $\|\boldsymbol{\theta}\| = 1$

$$\boldsymbol{\theta}(\varphi,\vartheta) = \begin{pmatrix} \cos(\varphi)\sin(\vartheta) \\ \sin(\varphi)\sin(\vartheta) \\ \cos(\vartheta) \end{pmatrix},$$

so that the vector $\boldsymbol{r} = r_l\,\boldsymbol{\theta}$ lies on the sphere.

Consider now continuously spread sources at this radius that excite the Helmholtz equation with a continuous distribution of source strength $f(\boldsymbol{\theta})$

$$\left(\Delta + k^2\right) p = -\frac{\delta(r - r_l)}{r^2}\, f(\boldsymbol{\theta}). \tag{1}$$

In this equation, $p$ represents the sound pressure, $\Delta$ the Laplace-operator, $\delta(r - r_l)$ a Dirac delta distribution and $k = \frac{2\pi}{\lambda}$ the wave-number, whereby $\lambda$ is the wave length, cf. [27, 37].

The nonhomogeneous Helmholtz equation, $f(\boldsymbol{\theta}) \neq 0$, is solved by seperation of variables, using a product Ansatz, cp. [37, 27]

$$p(kr,\boldsymbol{\theta}) = R(kr)\;\Phi(\boldsymbol{\theta}). \tag{2}$$

With the homogeneous and nonhomogeneous solutions of the Helmholtz equation in Appendix A, the complete solution of the spherical source strength distribution, i.e. its spherical harmonics transform representation $\phi_{nm}$

$$\phi_{nm} = \int_{\mathbb{S}^2} f(\boldsymbol{\theta})\; Y_n^m(\boldsymbol{\theta})\; d\boldsymbol{\theta}, \tag{3}$$

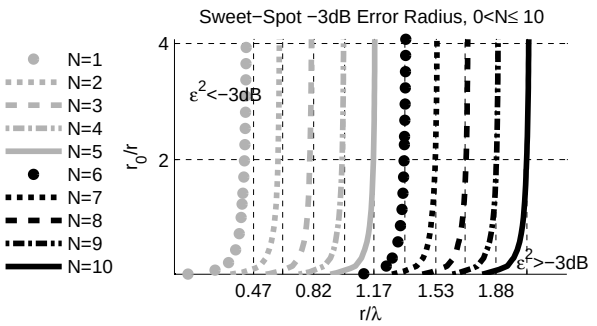


Fig. 3: −3dB border of the listening area in wave lengths, depending on the reproduction order N and the source radius $r_0$.

can be given as

$$p(kr,\boldsymbol{\theta}) = -\sum_{n=0}^{\infty}\sum_{m=-n}^{n} \mathrm{i}k\;\phi_{nm}\;Y_n^m(\boldsymbol{\theta})\cdot \cdot \begin{cases} h_n(kr_l)\;j_n(kr), & \text{for } r < r_l, \\ j_n(kr_l)\;h_n(kr), & \text{for } r > r_l. \end{cases} \tag{4}$$

For Ambisonics, only the first case is applicable.

## 4. FINITE-ORDER TRUNCATION ERROR

In [8, 6] the accuracy of the representation of plane-waves and point-sources using a truncated order $n \le \mathrm{N}$ has been given, depending on the radius of observation $r$. We present a compact form of the equation for point-sources and obtain a precise descriptor of the resynthesis error.

**Representation of a single point-source.** Inserting the spherical harmonics transform of an angular Dirac delta distribution $f(\boldsymbol{\theta}) = \delta(1 - \boldsymbol{\theta}^{\mathrm{T}}\boldsymbol{\theta}_0)$ pointing towards $\boldsymbol{\theta}_0$

$$\phi_{nm} = \int_{\mathbb{S}^2} \delta(1 - \boldsymbol{\theta}^{\mathrm{T}}\boldsymbol{\theta}_0) Y_n^m(\boldsymbol{\theta}) d\boldsymbol{\theta} = Y_n^m(\boldsymbol{\theta}_0), \tag{5}$$

into Eq. (4), yields the representation of a single point-source at $r_0 \ge r$,

$$G(\boldsymbol{r},\boldsymbol{r}_0) = -\mathrm{i}k\sum_{n=0}^{\infty}\sum_{m=-n}^{n} j_n(kr)h_n(kr_0)Y_n^m(\boldsymbol{\theta})\,Y_n^m(\boldsymbol{\theta}_0).$$

The normalized squared error assotiated with a point-source representation of finite order, as derived in Appendix B, yields

$$\epsilon^2 = 1 - \frac{2\,kr_0 kr}{\ln\left(\frac{r+r_0}{r-r_0}\right)} \sum_{n=0}^{\mathrm{N}} (2n+1)\ \left|j_n\left(kr\right) h_n\left(kr_0\right)\right|^2 . \tag{6}$$

Essentially, from Eq. (6) a radius in wave lengths $r/\lambda$ can be determinded, inside of which the resynthesis error does not exceed a given limit.

We define the area, within $20\,log_{10}(\epsilon) \le -3\mathrm{dB}$, as the sweet spot. This $-3$dB-limit does not refer to perceptive qualities, e.g. an audible threshold, but complies with well-known definitions of cut-off frequencies[2]. Fig. 3 shows the sweet spot radius as a function of the relative source distance $r_0/r$ for various orders N. As a rule of thumb, sources at $r_0/r \ge 2$ are well-modeled using the plane-waves sweet spot size, cp. [8].

## 5. MODAL SOURCE STRENGTH MATCHING

In order to reproduce $f(\boldsymbol{\theta})$, loudspeakers are placed at the set of discrete angles $\{\boldsymbol{\theta}_l\}$ with $l = 1, \ldots \mathrm{L}$, and driven by the gains $\{g_l\}$. Each of the loudspeakers is assumed to create the field of a point-source, which can be expressed as the nonhomogeneous Helmholtz-equation

$$(\Delta + k^2)\hat{p} = -\frac{\delta(r-r_l)}{r^2} \sum_{l=1}^{\mathrm{L}} g_l\ \delta(1 - \boldsymbol{\theta}^{\mathrm{T}}\boldsymbol{\theta}_l). \tag{7}$$

The continuous and the discretized angular source strength distributions $f(\boldsymbol{\theta})$ and $\hat{f}(\boldsymbol{\theta}) = \sum_{l=1}^{\mathrm{L}} g_l\ \delta(1 - \boldsymbol{\theta}^{\mathrm{T}}\boldsymbol{\theta}_l)$ on the right hand sides of Eqs. (1) and (7) can be compared directly

$$f(\boldsymbol{\theta}) \overset{!}{\approx} \hat{f}(\boldsymbol{\theta}), \tag{8}$$

which however is problematic, since angular information between the loudspeakers may get lost. Angular smoothing and matching in the modal angular harmonics domain prevents this loss of information.

[2]Below this limit the squared resynthesis error is smaller than half the squared desired field.

**Angular band-limitation.** Ideal angular low-pass filtering is denoted as $\mathcal{B}_{\mathrm{N}}\{\cdot\}$, here. It corresponds to a truncation of spherical harmonics orders $n > \mathrm{N}$. The comparison between the continuous and discretized angular source strength distribution, both at ideally smoothed resolution, remains what we refer to as *modal source strength matching*

$$\begin{aligned} \mathcal{B}_{\mathrm{N}}\left\{f(\boldsymbol{\theta})\right\} &\overset{!}{=}_{g_l} \sum_{l=1}^{\mathrm{L}} g_l\ \mathcal{B}_{\mathrm{N}}\left\{\delta(1-\boldsymbol{\theta}^{\mathrm{T}}\boldsymbol{\theta}_l)\right\}, \\ \phi_{nm} &\overset{!}{=}_{g_l} \sum_{l=1}^{\mathrm{L}} g_l\ Y_n^m(\boldsymbol{\theta}_l), \\ &\forall 0 \le n \le \mathrm{N}, -n \le m \le n. \end{aligned} \tag{9}$$

In order to solve the system of equations in Eq. (9), the *modal source strength matching approach* is usually reformulated in matrix notation.

**Matrix/vector notation.** The following conventions are introduced

$$\boldsymbol{\phi}_{\mathrm{N}} \overset{!}{=}_{\boldsymbol{g}} \underbrace{\boldsymbol{Y}_{\mathrm{N}}\,\boldsymbol{g}}_{\hat{\boldsymbol{\phi}}_{\mathrm{N}}}, \tag{10}$$

$$\begin{aligned} \text{with } \boldsymbol{Y}_{\mathrm{N}} &= \left(\boldsymbol{y}_{\mathrm{N}}(\boldsymbol{\theta}_1),\, \boldsymbol{y}_{\mathrm{N}}(\boldsymbol{\theta}_2),\, \ldots,\, \boldsymbol{y}_{\mathrm{N}}(\boldsymbol{\theta}_{\mathrm{L}})\right), \\ \boldsymbol{g} &= \left(g_1,\, g_2,\, \ldots,\, g_{\mathrm{L}}\right)^{\mathrm{T}}, \\ \boldsymbol{y}_{\mathrm{N}}(\boldsymbol{\theta}) &= \left(Y_0^0(\boldsymbol{\theta}), Y_1^{-1}(\boldsymbol{\theta}), Y_1^0(\boldsymbol{\theta}), Y_1^1(\boldsymbol{\theta}), \ldots, Y_{\mathrm{N}}^{\mathrm{N}}(\boldsymbol{\theta})\right)^{\mathrm{T}}, \\ \boldsymbol{\phi}_{\mathrm{N}} &= \left(\phi_{0,0},\, \phi_{1,-1},\, \phi_{1,0},\, \phi_{1,1}.\, \ldots,\, \phi_{\mathrm{N},\mathrm{N}}\right)^{\mathrm{T}}, \\ \mathrm{diag}_{\mathrm{N}}\left\{a_{nm}\right\} &= \mathrm{diag}\left\{\boldsymbol{a}_{\mathrm{N}}\right\}. \end{aligned}$$

### 5.1. Modal source strength matching

Eq. (10) represents the *modal source strength matching* equation in matrix/vector form. To match $\hat{\boldsymbol{\phi}}_{\mathrm{N}}$ to a desired modal source strength $\boldsymbol{\phi}_{\mathrm{N}} \overset{!}{=} \hat{\boldsymbol{\phi}}_{\mathrm{N}}$, a *decoder* matrix $\boldsymbol{D}_{\mathrm{N}}$ is introduced, which controls the speaker gains $\boldsymbol{g} = \boldsymbol{D}_{\mathrm{N}}\,\boldsymbol{\phi}_{\mathrm{N}}$. We obtain from Eq. (10) the smoothed reproduced modal source strength

$$\hat{\boldsymbol{\phi}}_{\mathrm{N}} = \boldsymbol{Y}_{\mathrm{N}}\,\boldsymbol{D}_{\mathrm{N}}\,\boldsymbol{\phi}_{\mathrm{N}}. \tag{11}$$

It matches exactly if $\boldsymbol{D}_{\mathrm{N}}$ is the right inverse of $\boldsymbol{Y}_{\mathrm{N}}$

$$\boldsymbol{D}_{\mathrm{N}} = \boldsymbol{Y}_{\mathrm{N}}^{\mathrm{T}}\left(\boldsymbol{Y}_{\mathrm{N}}\,\boldsymbol{Y}_{\mathrm{N}}^{\mathrm{T}}\right)^{-1}. \tag{12}$$

Note that *modal source strength matching* is well-conditioned as long as the right-inverse of $\boldsymbol{Y}_{\mathrm{N}}$ is, cf. [25]. It does not exhibit restricted frequencies as the *mode-matching approach*.

**Synthesis equation.** Eq. (4) in vector notation determines the resynthesized sound pressure

$$\hat{p}(kr,\boldsymbol{\theta}) = -\mathrm{i}k\,\boldsymbol{y}_{\mathrm{Q}}^{\mathrm{T}}(\boldsymbol{\theta})\,\mathrm{diag}_{\mathrm{Q}}\left\{j_n(kr)\,h_n(kr_l)\right\}\,\hat{\boldsymbol{\phi}}_{\mathrm{Q}}. \tag{13}$$

It uses the unsmoothed reproduced modal source strength

$$\hat{\boldsymbol{\phi}}_{\mathrm{Q}} = \boldsymbol{Y}_{\mathrm{Q}}\,\boldsymbol{D}_{\mathrm{N}}\,\boldsymbol{\phi}_{\mathrm{N}}. \tag{14}$$

Exploiting the orthonormality of the spherical harmonics, cf. [29],

$$\int_{\mathbb{S}^2} \boldsymbol{y}_{\mathrm{Q}}(\boldsymbol{\theta}_2)\,\boldsymbol{y}_{\mathrm{Q}}^{\mathrm{T}}(\boldsymbol{\theta}_2)\,d\boldsymbol{\theta}_2 = \boldsymbol{I}, \tag{15}$$

the resynthesis Eq. (13) transforms to the spherical harmoncis domain $\hat{\boldsymbol{\psi}}_{\mathrm{Q}}(kr) = \int_{\mathbb{S}^2} \boldsymbol{y}_{\mathrm{Q}}(\boldsymbol{\theta})\,\hat{p}(kr,\boldsymbol{\theta})\,d\boldsymbol{\theta}$, the *spherical wave spectrum* of the sound pressure, cf. [26],

$$\hat{\boldsymbol{\psi}}_{\mathrm{Q}}(kr) = -\mathrm{i}k\,\mathrm{diag}_{\mathrm{Q}}\left\{j_n(kr)\,h_n(kr_l)\right\}\boldsymbol{Y}_{\mathrm{Q}}\,\boldsymbol{D}_{\mathrm{N}}\,\boldsymbol{\phi}_{\mathrm{N}}. \tag{16}$$

For the sound pressure and its *spherical wave spectrum* the *Parseval theorem* holds, cf. [29],

$$\int_{\mathbb{S}^2} |\hat{p}(kr,\boldsymbol{\theta})|^2\,d\boldsymbol{\theta} \equiv \|\hat{\boldsymbol{\psi}}_{\mathrm{Q}}(kr)\|^2. \tag{17}$$

This theorem simplifies the analysis of the squared resynthesis error.

**Resynthesis error.** The synthesis error is the deviation of the resynthesized from the desired field

$$\boldsymbol{e}_{\mathrm{Q}} = \boldsymbol{\psi}_{\mathrm{Q}} - \hat{\boldsymbol{\psi}}_{\mathrm{Q}}. \tag{18}$$

Please note that $\boldsymbol{Y}_{\mathrm{Q}}\,\boldsymbol{D}_{\mathrm{N}} \neq \boldsymbol{I}$ in the resynthesis Eq. (16) readily contains the inherent spatial aliasing artifacts at the orders $\mathrm{N} < n \leq \mathrm{Q}$. Note again that for the orders $0 \leq n \leq \mathrm{N}$ synthesis is exact $\boldsymbol{e}_{\mathrm{N}} = \boldsymbol{0}$ if a decoder exists, fulfilling $\boldsymbol{Y}_{\mathrm{N}}\,\boldsymbol{D}_{\mathrm{N}} = \boldsymbol{I}$. However in common practise, angular band-limitation reproducing this portion of the spherical wave spectrum exclusively is not feasible for playback.

Usually, the desired modal source strength is chosen corresponding to a virtual point-source at the angle $\boldsymbol{\theta}_0$ and the radius $r_l$. According to Eq. (5) this is the low-order portion of $\boldsymbol{\phi}_{\mathrm{Q}} = \boldsymbol{y}_{\mathrm{Q}}(\boldsymbol{\theta}_0)$. The resynthesis error depends on the angular position $\boldsymbol{\theta}_0$ of a virtual point-source, the size $r_l$ of the playback facility, and the radius of observation $r$,

$$\boldsymbol{e}_{\mathrm{Q}} = \mathrm{i}k\,\mathrm{diag}_{\mathrm{Q}}\left\{j_n(kr)\,h_n(kr_l)\right\}\cdot \left[\boldsymbol{I} - \boldsymbol{Y}_{\mathrm{Q}}\,\left(\boldsymbol{D}_{\mathrm{N}},\,\boldsymbol{0}\right)\right]\boldsymbol{y}_{\mathrm{Q}}(\boldsymbol{\theta}_0). \tag{19}$$

The squared error is $\epsilon^2 = \|\boldsymbol{e}_{\mathrm{Q}}\|^2$.

Before starting a detailed analysis of the resynthesis error and spatial aliasing, *distance coding* [30, 31] is introduced to represent sources at variable radius $r_0 \neq r_l$.

## 6. SOURCE ENCODING WITH DISTANCE

Virtual radial scaling of the playback sphere, or *distance* coding, applies a useful trick: the radial function $h_n(kr_l)$ in Eq. (16) is compensated for by setting

$$\boldsymbol{\phi}_{\mathrm{N}} = \mathrm{diag}_{\mathrm{N}}\left\{\frac{h_n(kr_0)}{h_n(kr_l)}\right\}\tilde{\boldsymbol{\phi}}_{\mathrm{N}}. \tag{20}$$

At finite order $\mathrm{Q} = \mathrm{N}$, the term $\boldsymbol{Y}_{\mathrm{N}}\,\boldsymbol{D}_{\mathrm{N}}$ in Eq. (16) becomes the unity matrix. This achieves a replacement of $h_n(kr_l)$ by $h_n(kr_0)$,

$$\boldsymbol{\psi}_{\mathrm{N}}(kr) = -\mathrm{i}k\,\mathrm{diag}_{\mathrm{N}}\{j_n(kr)h_n(kr_0)\}\,\tilde{\phi}_{\mathrm{N}},$$

a virtual scaling of the radius of the playback facility.

**Spatial encoding of arbitrary point-sources.** A signal $s(\omega)$ is encoded into an Ambisonics signal $\boldsymbol{s}_{\mathrm{N}}(\omega)$ by multiplication with its desired modal source strength distribution $\boldsymbol{\phi}_{\mathrm{N}}$. To make it arrive from the direction $\boldsymbol{\theta}_0$, the we set $\boldsymbol{\phi}_{\mathrm{N}} = \boldsymbol{y}_{\mathrm{N}}(\boldsymbol{\theta}_0)$. From $\boldsymbol{s}_{\mathrm{N}}(\omega)$, the loudspeaker signals $\boldsymbol{x}(\omega)$ are obtained by the decoder $\boldsymbol{D}_{\mathrm{N}}$, cf. Eq. (12),

$$\boldsymbol{s}_{\mathrm{N}}(\omega) = \boldsymbol{y}_{\mathrm{N}}(\boldsymbol{\theta}_0)\;s(\omega) \tag{21}$$

$$\boldsymbol{x}(\omega) = \boldsymbol{D}_{\mathrm{N}}\,\boldsymbol{s}_{\mathrm{N}}(\omega). \tag{22}$$

Using radial scaling Eq. (20) for *distance coding* [30], the signal $s(\omega)$ encoded in both, angle and radius, is

$$\boldsymbol{s}_{\mathrm{N},\mathrm{r_{ref}}}(\omega) = \mathrm{diag}_{\mathrm{N}}\left\{\frac{h_n(kr_0)}{h_n(kr_{ref})}\right\}\boldsymbol{y}_{\mathrm{N}}(\boldsymbol{\theta}_0)\;s(\omega). \tag{23}$$

Note that the radius $r_{ref}$ is usually given by the size of the playback arrangement, and in principle limits the usability of the Ambisonics signal $\boldsymbol{s}_{\mathrm{N},\mathrm{r_{ref}}}(\omega)$ to this particular size.

However, a signal encoded for a given reference radius $r_{ref}$ can be adjusted to fit the actual radius $r_l$ of the playback facility using *distance coding* twice

$$\boldsymbol{s}_{\mathrm{N,r_l}}(\omega) = \mathrm{diag_N}\left\{\frac{h_n(kr_{ref})}{h_n(kr_l)}\right\}\boldsymbol{s}_{\mathrm{N,r_{ref}}}(\omega). \quad (24)$$

## 7. THE EFFECT OF ANGULAR ALIASING ON AMBISONICS

Using distance coding, the error measure considered in Eq. (19) can be extended to allow for virtual point-sources at arbitrary radius. As derived in Appendix B, the extended normalized squared error yields

$$\epsilon^2 = \frac{8\pi\, kr_0 kr}{\ln\left(\frac{r+r_0}{r-r_0}\right)} \sum_{n=\mathrm{N}+1}^{\infty} \sum_{m=-n}^{n} |e_{nm}|^2\,, \quad (25)$$

with

$$e_{nm} = j_n\,(kr)\left[h_n(kr_0)\,Y_n^m(\boldsymbol{\theta}_0) - h_n\,(kr_l)\sum_{l=1}^{\mathrm{L}} Y_n^m(\boldsymbol{\theta}_l)\,\boldsymbol{d}_l^{\mathrm{T}}\mathrm{diag_N}\left\{\frac{h_{n'}\,(kr_0)}{h_{n'}\,(kr_l)}\right\}\boldsymbol{y}_{\mathrm{N}}(\boldsymbol{\theta}_0)\right],$$

and $\boldsymbol{d}_l^{\mathrm{T}}$ representing the $l^{th}$ row of the decoder matrix $\boldsymbol{D}_{\mathrm{N}}$, cf. Eq. (12).

In comparison to Eq. (6), the extended error measure in Eq. (25) exhibits new dependencies on the angle of the virtual point-source $\boldsymbol{\theta}_0$, and the loudspeaker layout $r_l\,\{\boldsymbol{\theta}_l\}$. To carry out a thourough case study on the resythesis error for a loudspeaker layout, we are forced to specify the set of angular positions $\{\boldsymbol{\theta}_l\}$.

**Hyperinterpolation as loudspeaker layout.** In order to simulate spatial aliasing, *hyperinterpolation* has been chosen as angular sampling stragegy for the loudspeaker layout $\{\boldsymbol{\theta}_l\}$, see [32]. This choice has been made as it is expected to yield a *worst-case scenario* in terms of spatial aliasing. The fact that *hyperinterpolation* uses the smallest posible number of loudspeakers $\mathrm{L} = (\mathrm{N}+1)^2$, leads us to this expectation. As best case, however, decoding of a point-source coinciding with one of the speakers, e.g. the first one $\boldsymbol{r}_0 = r_l\boldsymbol{\theta}_1$, yields a non-zero signal for this particular speaker, only. This corresponds to the exact resynthesis of a point-source, which looks favorable at first sight, but might disturb the smooth resynthesis of Ambisonics playback.

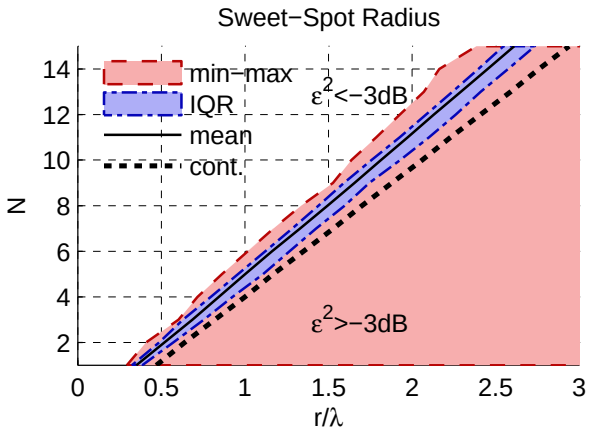


Fig. 4: Overview of the −3dB sweet-spot size in wave lengths for varying order $1 \le \mathrm{N} \le 15$ and relative distances $r_l/r = r_0/r_l = 50$. The diagram shows that the average, 25-75-IQR, and minmax-range of the sweet-spot size allow for a linear approximation. The black dashed line (labeled *cont*) marks the sweet-spot size for pure finite-order truncation.

**Spiral points for virtual point-source positions.** To reduce the analysis of the synthesis error by the dimension of the virtual source angle $\boldsymbol{\theta}_0$, statistical parameters are obtained from a set of 1000 angles $\{\boldsymbol{\theta}_0\}$. As a sampling strategy for these angles, the spiral points have been chosen, cf. [33]. These points nearly uniformly cover the sphere, which enables a consistent estimation of a mean square error. In the simulation, only one of these points coincides with a *hyperinterpolation* node. This particular point achieves a minimum resynthesis error of $\epsilon^2 = 0$ (see *hyperinterpolation*).

**Example 1: Contours at $r_l/r, r_0/r = 50$.** The first simulation of the spatial resynthesis errors with Eq. (25), uses a fixed constellation $r_l = r_0$, $r_0/r = 50$ of source and playback radius. The −3dB transition of the error along the normalized radius of

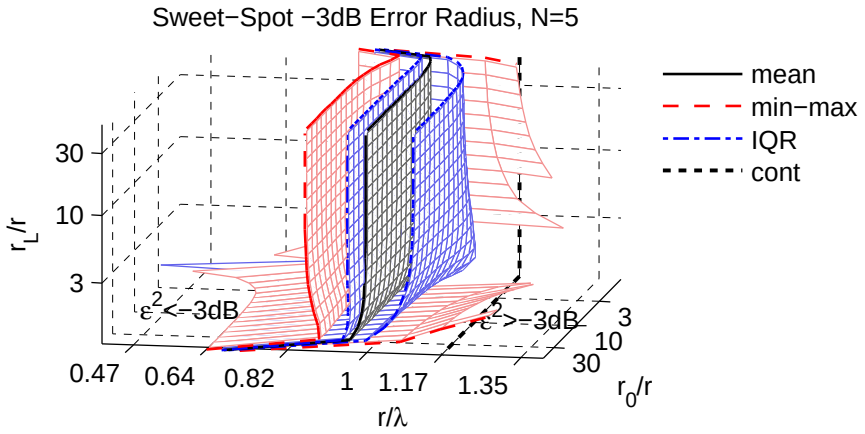


Fig. 5: The contours indicate the −3dB sweet-spot size in terms of $r/\lambda$ in its average, 25-75-IQR, and min-max range for a playback order of N = 5. The dashed black line on the floor and back plane (labeled *cont*) shows the −3dB sweet-spot size of pure finite-order truncation error without spatial aliasing.

observation $r/\lambda$, our definition of the sweet spot size, has been simulated for the orders $1 \le \mathrm{N} \le 15$. Fig. 4 shows the statistics of the sweet spot size, and indicates its average, 25%-75%-inter-quartile-range (IQR), and min-max range. In most cases, spatial aliasing decreases (and modulates) sweet spot size in comparison with its pure finite-order truncation size. Only for the exception that the virtual point-source position coincides with a loudspeaker position, the sweet spot size increases (see *hyperinterpolation*).

**Example 2: Contours for N=5.** The second simulation illustrates the dependency of the sweet spot size on the normalized radius of the loudspeaker layout $r_l/r$, and the virtual point-source $r_0/r$ for the order N = 5. Fig. 5 shows the statistics of the sweet spot size, i.e. indicates its average, the 25-75-IQR, and the min-max range. As a rule of thumb, for $r_0/r, r_l/r \ge 2$, the transition radius asymptotically stalls at a constant value. Again, the sweet spot is exceptionally large for the virtual source position that coincides with a loudspeaker position (see *hyperinterpolation*).

## 8. CONCLUSION

In this paper we have shown an alternative formulation of Ambisonics by directly solving the nonhomogeneous Helmholtz-equation and introducing the concept of *modal source strength matching*, which does not suffer from ill-conditioning.

It does not withdraw a simple interpretation of Ambisonics without *distance coding*. Therein the playback loudspeaker arrangement is used to reproduce virtual point-sources at the surface it spans. For this purpose, only real-valued frequency-independent gains are required.

It also demonstrates the influence of finite angular resolution (order truncation) and spatial aliasing on the resynthesis error, successively. To this end, the synthesis error has been compactly reformulated, covering also *distance coding* of virtual point-sources.

A thourough case study has been carried out, which investigates the dependency of the sweet spot size on the playback order, the size of the playback arrangement, and the position of a virtual point-source. Clever normalization allows to summarize the essential outcome of this study in few diagrams. However, the given definition of the sweet spot size is purely mathematical, hence does not cover perceptive aspects. Evaluation of the preceived synthesis accuracy requires dedicated listening tests, cf. [34, 35].

## 9. ACKNOWLEDGEMENTS

We gratefully thank Jens Ahrens for his encouragement to write this paper and discussion, as well as

Filippo Fazi for his critical comments. This work was partly funded by the Austrian Research Promotion Agency, Prj. 815085.

## 10. REFERENCES

[1] G. Theile, "On the Performance of Two-Channel and Multi-Channel Stereophony," presented at the AES 88th convention, Montreux, March 13–16, 1990.

[2] V. Pulkki, "Virtual Sound Source Positioning Using Vector Base Amplitude Panning," JAES Volume 45 Issue 6 pp. 456–466; June 1997.

[3] J. Blauert, "Spatial Hearing - The Psychophysics of Human Sound Localization," The MIT-Press, Cambridge, MA; 1983.

[4] M. A. Gerzon, "Periophony (With-heigth sound reproduction)," presented at the AES 2CE Convention, Munich, March 14–16, 1972.

[5] J.Daniel., "Représentation de champs acoustiques, application à la transmission et à la reproduction de scénes sonores complexes dans un contexte multimédia," PhD thesis, Université de Paris 6, 2001.

[6] M. A. Poletti, "Three-Dimensional Surround Sound Systems Based on Spherical Harmonics," JAES Volume 53 Issue 11 pp. 1004–1025, November 2005.

[7] J. Ahrens and S. Spors, "An Analytical Approach to Sound Field Reproduction Using Circular and Spherical Loudspeaker Distributions," Acta Acustica united with Acustica, Volume 94, Number 6, pp. 988–999, November–December, Hirzel Verlag, 2008.

[8] D. Ward and T. Abhayapala, "Reproduction of a plane-wave sound field using an array of loudspeakers," IEEE Transactions on Speech and Audio Processing, 9, 697–707, 2001.

[9] F. Fazi et al., "Surround System Based on Three-Dimensional Sound Field Reconstruction," presented at the AES 125th Convention, San Francisco, USA, October 2-5, 2008.

[10] S. Moreau, "Étude et réalisation d'outils avancés d'encodage spatial pour la technique de spatialisation sonore Higher Order Ambisonics: microphone 3D et contrôle de distance," PhD thesis, Université du Maine, 2006.

[11] J. Ahrens and S. Spors, "Rendering of Virtual Sound Sources with Arbitrary Directivity in Higher Order Ambisonics," presented at the AES 123rd Convention, New York, October 5-8, 2007.

[12] J. Meyer, and G. Elko, "A highly scalable spherical microphone array based on an orthonormal decomposition of the soundfield," Proc. IEEE ICASSP(2), 2002.

[13] B. Rafaely, B. Weiss, and E. Bachmat, "Spatial Aliasing in Spherical Microphone Arrays," IEEE Transactions on Signal Processing, 55(3), 2007.

[14] Z. Li, "The Capture and Recreation of 3D Audio Scenes," PhD thesis, University of Maryland, 2005.

[15] S.-O. Petersen, "Localization of Sound Sources Using 3D Microphone Array," M. thesis, University South Denmark, Odense, 2004.

[16] W. Song, W. Ellermeier, and J. Hald, "Using beamforming and binaural synthesis for the psychoacoustical evaluation of target sources in noise," JASA, no. 123, pp. 910–924, 2008.

[17] O. Warusfel, P. Derogis, and R. Caussé, "Radiation Synthesis with Digitally Controlled Loudspeakers," 103rd AES Convention, New York, 1997.

[18] Franz Zotter and Robert Höldrich, "Modeling Radiation Synthesis with Spherical Loudspeaker Arrays," Proc. 19th ICA, Madrid, 2007.

[19] Franz Zotter, "Directional recording and analysis of sounds from musical instruments," Acoustics08, talk, Paris, 2008.

[20] M. Pollow, "Variable Directivity of Dodecahedron Loudspeakers," M. thesis, ITA, RWTH-Aachen, 2007

[21] H. Pomberger, "Angular and Radial Directivity Control for Spherical Loudspeaker Arrays," M. thesis, IEM,TU-Graz, 2008.

[22] J. S. Bamford and J. Vanderkooy, "Ambisonic Sound for Us (An Analysis of Imaging in Ambisonics, Stereo and Dolby Surround Systems)," presented at the AES 99th Convention, New York, October 6–9, 1995.

[23] S. Spors and J. Ahrens, "A Comparison of Wave Field Synthesis and Higher-Order Ambisonics with Respect to Physical Properties and Spatial Sampling," presented at the AES 125th Convention, San Francisco, CA, USA, October 2-5, 2008.

[24] Y. J. Wu and T. D. Abhayapala, "Soundfield reproduction using theoretical continuous loudspeaker," IEEE International Conference on Acoustics, Speech and Signal Processing, pp. 377–380, March 31 – April 4, 2008.

[25] Franz Zotter, "Characterization of Sampling Strategies on the Sphere," NAG-DAGA, Rotterdam, 2009.

[26] E. G. Williams, "Fourier Acoustics," Academic Press, 1999

[27] P. M. Morse and H. Feshbach, "Methods of Theoretical Physics," Part I&II, McGraw-Hill, 1953.

[28] F. M. Fazi, P. A. Nelson, "The ill-conditioning problem in Sound Field Reconstrution," 123rd AES Convention, New York, 2007.

[29] N. A. Gumerov and R. Duraiswami, "Fast Multipole Methods for the Helmholtz Equations in Three Dimensions," Elsevier, 1st ed., 2004.

[30] J. Daniel, "Spatial Sound Encoding Including Near Field Effect: Introducing Distance Coding Filters and a Viable, New Ambisonic Format," presented at the AES 23rd Conference, Copenhagen, Denmark, May 23–25, 2003.

[31] A. Sontacchi and R. Höldrich, "Distance Coding in 3D Sound Fields," presented at the AES 21st Conference, St. Petersburg, Russia, June 1-3, 2002.

[32] R. S. Womersley and I. H. Sloan, "How Good can Polynomial Interpolation on the Sphere be?," School of Mathematics, University New South Wales, Sydney, 2001.

[33] E. A. Rakhmanov, E. B. Saff, and Y. M. Zhou, "Minimal Discrete Energy on the Sphere," Mathematical Research Letters, 1994.

[34] M. Frank et al., "Localization Experiments Using Different 2D Ambisonics Decoders," presented at the 25th Tonmeistertagung, Leizig, 2008.

[35] S. Bertet et al., "Investigation of the perceived spatial resolution of higher order Ambisonics sound fields: a subjective evaluation involfing virtual and real 3D microphones," presented at the 23rd AES Conference, 2007.

[36] L. J. Ziomek, "Fundamentals of Acoustic Field Theory and Space-Time Singal Processing," CRC Press, 1995.

[37] E. Kreyszig, "Advanced Engineering Mathematics," Wiley, 8th ed., 1999.

## APPENDIX A

This appendix describes the homogeneous and nonhomogeneous solution of the Helmholtz equation Eq. (1).

**Homogeneous solutions.** In the spherical coordinate system, the Helmholtz equation yields the following base solutions, cf. [27, 29, 36, 26]

$$p_h(kr,\boldsymbol{\theta}) = Y_n^m(\boldsymbol{\theta}) \begin{cases} j_n(kr), & \text{incident field} \\ h_n(kr), & \text{radiating field.} \end{cases} \tag{26}$$

with $n,m \in \mathbb{Z} : n \geq 0, -n \geq m \geq n$. The real-valued spherical harmonics $Y_n^m(\boldsymbol{\theta})$ are the harmonic solutions for the angular part, and the radial part is solved by the spherical Bessel and Hankel functions $j_n(kr)$, $h_n(kr)$ , cf. [36, 26]. Note that all admissible solutions must take the form of Eq. (26) or weighted sums thereof.

**Nonhomogeneous solution.** According to Eq. (2), the angular part $\Phi(\boldsymbol{\theta})$ is easily described by the spherical harmonics transform pair of the source strength $f(\boldsymbol{\theta})$

$$\phi_{nm} = \int_{\mathbb{S}^2} f(\boldsymbol{\theta})\, Y_n^m(\boldsymbol{\theta})\, d\boldsymbol{\theta},$$
$$f(\boldsymbol{\theta}) = \sum_{n=0}^{\infty} \sum_{m=-n}^{n} \phi_{nm}\, Y_n^m(\boldsymbol{\theta}),$$

hence the solution for one of the harmonics becomes

$$p(kr,\boldsymbol{\theta}) = R(kr)\, \phi_{nm}\, Y_n^m(\boldsymbol{\theta}). \tag{27}$$

With the Laplace operator split up into its radial and angular part $\Delta = \Delta_r + \Delta_{\boldsymbol{\theta}}$, and the angular Eigenvalues and Eigenfunctions $\Delta_{\boldsymbol{\theta}} Y_n^m(\boldsymbol{\theta}) = -\frac{n(n+1)}{r^2}\, Y_n^m(\boldsymbol{\theta})$, the insertion of the Ansatz results in a nonhomogeneous, one-dimensional spherical Bessel differential equation, cf. [27],

$$\left[\Delta_r + k^2 - \frac{n(n+1)}{r^2}\right] R(kr) = -\frac{\delta(r-r_l)}{r^2}. \tag{28}$$

Since two independent homogeneous solutions $j_n(kr)$, and $h_n(kr)$ solve the above differential equation, the nonhomogeneous radial part $R(kr)$ is solved by *variation of parameters*, cf. [37]

$$R(kr) = -j_n(kr) \int_r^{\infty} \frac{h_n(kr)}{W(kr)} \frac{\delta(r-r_l)}{r^2} \frac{dkr}{k} - h_n(kr) \int_0^{r} \frac{j_n(kr)}{W(kr)} \frac{\delta(r-r_l)}{r^2} \frac{dkr}{k}, \tag{29}$$

wherein

$$W(kr) = \begin{vmatrix} j_n(kr) & h_n(kr) \\ j_n'(kr) & h_n'(kr) \end{vmatrix} = \frac{1}{\mathrm{i}(kr)^2}$$

is the Wronski-determinant, cf. [37, 29], of the two solutions. The result is given in Eq. (4).

## APPENDIX B

A normalized error measure for finite-order synthesis of a point-source can be found in analogy to [8] as

$$\epsilon^2 = \frac{\int_{\mathbb{S}^2} \left|G(\boldsymbol{r}_1,\boldsymbol{r}_2) - p(kr_1,\boldsymbol{\theta}_1)\right|^2 d\boldsymbol{\theta}_1}{\eta^2}. \tag{30}$$

A Green's function (point-source) in Cartesian and spherical coordinates is described as

$$G(\boldsymbol{r}_1,\boldsymbol{r}_2) = \frac{e^{-\mathrm{i}k\|\boldsymbol{r}_1-\boldsymbol{r}_2\|}}{4\pi\,\|\boldsymbol{r}_1-\boldsymbol{r}_2\|} \tag{31}$$
$$= \frac{k}{\mathrm{i}} \sum_{n=0}^{\infty} \sum_{m-n}^{n} j_n(kr_1) h_n(kr_2) Y_n^m(\boldsymbol{\theta}_1)\, Y_n^m(\boldsymbol{\theta}_2),$$
$$\text{with } \boldsymbol{r}_1 = r_1\,\boldsymbol{\theta}_1,$$
$$\boldsymbol{r}_2 = r_2\,\boldsymbol{\theta}_1,$$
$$\text{and } r_1 \leq r_2.$$

For the normalization term $\eta^2$, the surface integral of the absolute-squared point-source over a sphere requires evaluation

$$\eta^2 = \frac{1}{(4\pi)^2} \int_{\mathbb{S}^2} \frac{d\boldsymbol{\theta}_1}{\|\boldsymbol{r}_1-\boldsymbol{r}_2\|^2},$$

and simplifies to

$$\eta^2 = \frac{\int_0^{2\pi} d\varphi}{(4\pi)^2} \int_{-1}^{1} \frac{d\mu_1}{r_1^2+r_2^2-2r_1r_2\mu_1}, = \frac{\ln\left(\frac{r_1+r_2}{r_2-r_1}\right)}{8\pi r_1 r_2}, \tag{32}$$

using the surface element $d\boldsymbol{\theta}_1 = d\mu_1\, d\varphi$, $\mu_1 = \cos(\vartheta_1)$, and assuming $r_1 = \|\boldsymbol{r}_1\|$, and $\boldsymbol{r}_2 = (0,\ 0,\ r_2)^{\mathrm{T}}$.

Using the *Parseval theorem*, Eq. (17), to calculate the same within the *spherical wave spectrum*, see Eq. (31), with $\boldsymbol{\theta}_2 = \boldsymbol{\imath}_z = (0,\, 0,\, 1)^{\mathrm{T}}$ and $r_2$, yields (see also [8, 6])

$$\eta_{\mathrm{Q}}^2 = k^2 \| \mathrm{diag}_{\mathrm{Q}}\{j_n(kr_1) h_n(kr_2)\}\, \boldsymbol{y}_{\mathrm{Q}}(\boldsymbol{\imath}_z)\, \|^2. \quad (33)$$

Note that the latter formulation allows for a reduction of the order $\mathrm{Q} \to \infty$ to a finite value N.

**Finite-order truncation.** As for the truncation error, the truncated components of the *spherical wave spectrum* do not mix in the vector norm, it may be re-written as:

$$\epsilon^2 = \frac{\eta^2 - k^2 \| \mathrm{diag}_{\mathrm{N}}\{j_n(kr_1) h_n(kr_2)\}\, \boldsymbol{y}_{\mathrm{N}}(\boldsymbol{\imath}_z)\, \|^2}{\eta^2}. \quad (34)$$

With the spherical harmonics addition theorem [29] $\boldsymbol{y}_{\mathrm{N}}(\boldsymbol{\imath}_z)\, \boldsymbol{y}_{\mathrm{N}}^{\mathrm{T}}(\boldsymbol{\imath}_z) = \mathrm{diag}_{\mathrm{N}} \left\{ \frac{2n+1}{4\pi} \delta_m \right\}$, this equation exactly corresponds to Eq. (6).

**Error with spatial aliasing.** Spatial aliasing makes the error dependent on the position of the virtual source, thus does not allow selection of a fixed position. However a probe for one specific virtual point-source position $r_2\, \boldsymbol{\theta}_2$ may be taken

$$\epsilon^2 = \frac{k^2}{\eta^2} \Big\| \mathrm{diag}_{\mathrm{N}}\{j_n(kr_1) h_n(kr_2)\} \cdot \left[ \boldsymbol{I} - \boldsymbol{Y}_{\mathrm{Q}}\, \left( \boldsymbol{D}_{\mathrm{N}},\, \boldsymbol{0} \right) \right]\, \boldsymbol{y}_{\mathrm{Q}}(\boldsymbol{\theta}_2) \Big\|^2. \quad (35)$$

Using *distance coding* for playback loudspeakers at the radius $r_3$, the expression gets more complex

$$\epsilon^2 = \frac{k^2}{\eta^2} \Big\| \mathrm{diag}_{\mathrm{N}}\{j_n(kr_1)\} \cdot \Big[ \mathrm{diag}_{\mathrm{Q}}\{h_n(kr_2)\} - \mathrm{diag}_{\mathrm{Q}}\{h_n(kr_3)\} \cdot \boldsymbol{Y}_{\mathrm{Q}}\, \boldsymbol{D}_{\mathrm{N}} \left( \mathrm{diag}_{\mathrm{N}} \left\{ \frac{h_n(kr_2)}{h_n(kr_3)} \right\},\, \boldsymbol{0} \right) \Big]\, \boldsymbol{y}_{\mathrm{Q}}(\boldsymbol{\theta}_2) \Big\|^2. \quad (36)$$

**Average error.** Despite the dependency of the error on the choice of the virtual point-source position $r_2\, \boldsymbol{\theta}_2$, an analytic calculation of its average is feasible. Using an integral over all virtual source positions, the property $\|\boldsymbol{e}_{\mathrm{Q}}\|^2 = \boldsymbol{e}_{\mathrm{Q}}^{\mathrm{H}} \boldsymbol{e}_{\mathrm{Q}} = \mathrm{Tr}\{\boldsymbol{e}_{\mathrm{Q}} \boldsymbol{e}_{\mathrm{Q}}^{\mathrm{H}}\}$ and the orthonormality of the spherical harmonics, Eq. (15), can be exploited. Hereby, the average is obtained by replacing the desired modal source strength $\boldsymbol{y}_{\mathrm{Q}}(\boldsymbol{\theta}_2)$ with a scaled vector of ones $\frac{1}{\sqrt{4\pi}}\, \boldsymbol{1} = \frac{1}{\sqrt{4\pi}} (1,\, \ldots\, , 1)^{\mathrm{T}}$ in the above equations.